ADVANCED MATERIALS
www.advmat.de

Conformation Dynamics of Single Polymer Strands in Solution

Yuna Bae, Min Young Ha, Ki-Taek Bang, Sanghee Yang, Sung Yun Kang, Joodeok Kim, Jongbaek Sung, Sungsu Kang, Dohun Kang, Won Bo Lee, Tae-Lim Choi,* and Jungwon Park**

Conformational changes in macromolecules significantly affect their functions and assembly into high-level structures. Despite advances in theoretical and experimental studies, investigations into the intrinsic conformational variations and dynamic motions of single macromolecules remain challenging. Here, liquid-phase transmission electron microscopy enables the real-time tracking of single-chain polymers. Imaging linear polymers, synthetically dendronized with conjugated aromatic groups, in organic solvent confined within graphene liquid cells, directly exhibits chain-resolved conformational dynamics of individual semiflexible polymers. These experimental and theoretical analyses reveal that the dynamic conformational transitions of the single-chain polymer originate from the degree of intrachain interactions. In situ observations also show that such dynamics of the single-chain polymer are significantly affected by environmental factors, including surfaces and interfaces.

1. Introduction

Macromolecules possess chain structures composed of repeating building blocks and show different degree of the flexibility in solution. In various solution systems of biological and synthetic polymers, macromolecules exist in a range of distinct conformations, shifting between them via dynamic transitions.[1–3] Thus, these dynamic motions dictate the specific functions and physicochemical properties of macromolecules, as well as the pathways toward their assembly into high-level structures. For example, intrinsically disordered proteins, which account for one-third of the proteins in the human proteome, do not adopt a standardized 3D structure, and their spontaneous interconversion between unfolded states is crucial in dynamic biological processes.[4] In addition, various synthetic polymers, which are highly regulated by complex molecular interactions and the resulting conformational changes, form a variety of high-order structures via the self-structuring of individual molecules.[5–8] Thus, it is important to understand the intrinsic structural diversity and dynamic behaviors of individual macromolecules at the single-chain level.

Over the last few decades, the conformation and dynamics of a single chain have been widely studied both theoretically and experimentally. Theoretical and computational modeling of single-chain dynamics in ideal solutions are well established in the field of polymer physics.[9–12] Moreover, enhanced sampling simulation techniques can efficiently locate candidates for energetically stable structures and calculate the free energy differences between their distinct states.[13–15] Nonetheless, it is still challenging to understand realistic single-chain behaviors using computational methods, as it is not trivial to simulate ion–solute interactions, crowding, or confinement in polymer solutions.[16–18] Furthermore, it is not rare to find a

Y. Bae, M. Y. Ha, J. Kim, J. Sung, S. Kang, W. B. Lee, J. Park
School of Chemical and Biological Engineering
Seoul National University
Seoul 08826, Republic of Korea
E-mail: wblee@snu.ac.kr; jungwonpark@snu.ac.kr

Y. Bae, J. Kim, J. Sung, S. Kang, J. Park
Institute of Chemical Processes
Seoul National University
Seoul 08826, Republic of Korea

Y. Bae, J. Kim, J. Sung, S. Kang, J. Park
Center for Nanoparticle Research
Institute for Basic Science (IBS)
Seoul 08826, Republic of Korea

The ORCID identification number(s) for the author(s) of this article can be found under https://doi.org/10.1002/adma.202202353.

DOI: 10.1002/adma.202202353

K.-T. Bang, S. Yang, S. Y. Kang, T.-L. Choi
Department of Chemistry
Seoul National University
Seoul 08826, Republic of Korea
E-mail: tlc@snu.ac.kr

D. Kang
Department of Materials Science and Engineering
Northwestern University
Evanston, IL 60208, USA

J. Park
Institute of Engineering Research
Seoul National University
Seoul 08826, Republic of Korea

J. Park
Advanced Institutes of Convergence Technology
Seoul National University
Suwon, Gyeonggi 16229, Republic of Korea

large gap in the time scale between theoretical predictions and realistic events occurring in polymer solutions.[19] The direct visualization of individual macromolecules and their structural dynamics has been experimentally attempted using single-molecule techniques. Atomic force microscopy (AFM) resolves polymer structures in solutions with sufficient contrast and spatial resolution, but it relies on the observation of adsorbed molecules.[20,21] In another approach, single-molecule fluorescence microscopy (SMFM) has been used to track the diffusion behaviors of various synthetic polymers and DNA strands based on the captured motions of labeled fluorescent molecules.[22–26] However, SMFM has an inherent limitation in achieving the sufficiently high spatial and temporal resolution required for investigating sub-molecular details of diffusing polymer chains.

Liquid-phase transmission electron microscopy (LPTEM) has recently enabled the direct observation of polymers, such as flexible polystyrene sulfonate and poly(ethylene oxide), in aqueous solutions.[27] It provides nanometer resolution for tracking individual molecules with random coil conformations in solution. Advancing LPTEM, here we achieve the high-resolution tracking of rigidified dendronized linear polymer chains in graphene liquid cell TEM, and elucidate the distinct individual chain architectures and conformational fluctuations of a single semiflexible polymer in organic solvent. Investigations of single-chain dynamics combined with molecular dynamics (MD) simulations directly reveal that the degree of intrachain interactions induces dynamic structural fluctuations between the coiled and elongated conformations of semiflexible polymers. Additionally, diverse single-chain behaviors, such as pinned motion, chain-scission, and even non-equilibrium single-chain motions, are observed. This shows that single-chain trajectories can be highly affected by the local heterogeneous environment.

2. Results and Discussion

2.1. Direct Observation of a Single Polymer Chain in a Graphene Liquid Cell

A graphene liquid cell is used to image the single-chain dynamics of linear polymers in their native solutions (**Figure 1**a). Using graphene as a window reduces the detrimental beam damage, which has been an issue plaguing the LPTEM analysis of soft materials such as polymers and biomolecules.[28–30] We encapsulate and image a synthetic polymer, the second-generation dendronized polymer, PTD–MuG2, consisting of poly(*endo*-tricyclo[4.2.2.0]deca-3,9-diene) (PTD) backbones and Müllen dendrons (Figure 1a). PTD–MuG2 is prepared by ring-opening metathesis polymerization (ROMP) (Supporting Information).[31,32] This polymer has numerous aromatic groups, enhancing its resistance to electron-beam-induced radiolysis during imaging.[33] More importantly, the high electron density of its bulky conjugated aromatic dendrons provides high contrast for the chain-resolved monitoring of single polymer strands via LPTEM. The synthesized polymer has been characterized by static light scattering (SLS), dynamic light scattering (DLS), and cryogenic transmission electron microscopy (cryo-TEM) (Figure 1b–d). The slope of the Debye plot for the dilute regime measured by SLS is used to estimate the second virial coefficient A_2, reflecting the solvent conditions. The near-zero A_2 value of PTD–MuG2 in toluene indicates that the polymer solution is in dilute theta conditions (Figure 1b). The hydrodynamic diameter of PTD–MuG2 with a molecular weight (M_n) of 490 kDa is ≈ 19.3 nm, as estimated by DLS (Figure 1c). Cryo-TEM, dry-state TEM, and AFM observations reveal the existence of PTD–MuG2 with various single-chain conformations under theta conditions in three organic solvents (Figure 1d; Figure S1 and Table S1, Supporting Information).

An in situ LPTEM movie of a single linear polymer in a dilute toluene solution (0.0001 mg mL^{-1}) displays dynamic conformational fluctuations of the polymer chain (Figure 1e; Movie S1, Supporting Information). From the projected chain contours of the TEM movie, the coordinates of the chain contours, contour lengths ($L_{c,proj.}$), and the center-of-mass position are directly tracked as a function of time over a period of 118 s (Supporting Information). This allows for the quantitative analysis of the conformational changes and dynamic motions of individual chains. The maximum contour length of the observed chain is about 55.4 nm, which is consistent with the expected length (57 nm) of the synthesized polymer with the number-average degree of polymerization (DP_n) of 153. The center-of-mass trajectories of a PTD–MuG2 chain show the diffusive behavior of Brownian motion with reduced diffusivity (Figure 1f; Figure S2, Supporting Information; see discussions for confinement effects in Sections S4 and S5, Supporting Information).[34,35] The superimposed trajectories of the chain contours indicate random fluctuations in their conformation (Figure 1g). The squared radius of gyration ($R_{g,proj.}^2$) of the chain that provides information on the compactness and the size of the PTD–MuG2 chain is calculated over time from the coordinates of the chain contours, showing dynamic conformational changes (Figure 1h and Figure S3, Supporting Information). The conformational relaxation time estimated from the autocorrelation function of the $R_{g,proj.}^2$ plot in Figure 1h is ≈ 1.59 s (Figure 1i; see discussions for slow dynamics in confined environments in Section S4, Supporting Information). It is worth noting that the subsecond temporal averaging (0.13 s) in the in situ LPTEM technique used in this study is optimized for the observation of the backbone conformational dynamics. Given that the relaxation time of the radius of gyration is 1.59 s (Figure 1i), a temporal averaging of 0.13 s is sufficient to cancel out the noisy motions of the dendrons while highlighting the main mode of the backbone dynamics.

2.2. Conformational Dynamics of Semi-Flexible Chains in a Graphene Liquid Cell

The detailed conformational changes and segmental dynamics of the PTD–MuG2 chain are clearly resolved in the LPTEM movie (Movie S1, Supporting Information). The polymer conformation dynamically changes between coiled and elongated shapes (Figure 1h; and Movie S1, Supporting Information) and exhibits distinct conformations with varying looped shapes containing zero to four loops (**Figure 2**a). These loop-like conformations are also observed in other solvents, such as chloroform

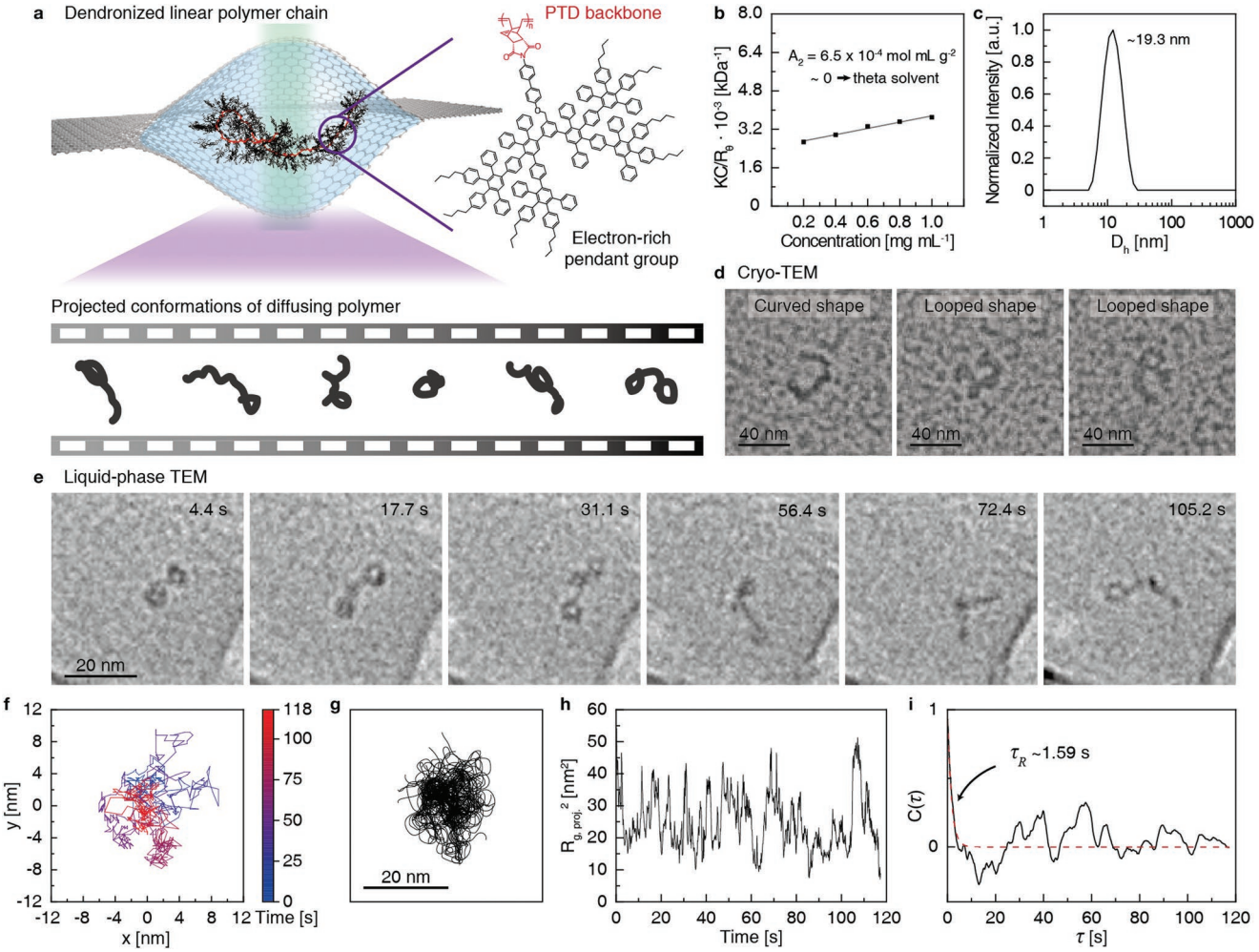

Figure 1. LPTEM imaging of a single polymer chain in a graphene liquid cell. a) Top: Schematic of a second-generation dendronized polymer (PTD–MuG2) encapsulated in a graphene liquid cell, whose PTD backbone carries Müllen dendrons. Bottom: A schematic movie of the projected conformations of a diffusing single polymer chain. b) Debye plot as a function of PTD–MuG2 concentration in toluene, showing that toluene is a theta solvent for PTD–MuG2. c) Chain hydrodynamic diameter distribution of PTD–MuG2 in toluene inferred from DLS with average diameter as shown. d) Cryo-TEM images showing the various morphologies of PTD–MuG2 in toluene ice. e) Time-series of LPTEM images for diffusing PTD–MuG2 in dilute toluene solutions (0.0001 mg mL^{-1}). f,g) Superimposed trajectories of the center-of-mass positions (f) and chain contours (g) of PTD–MuG2 in dilute toluene solutions over 118 s. h) The radius of gyration ($R_{g,proj.}^2$) over time and i) its autocorrelation function ($C(\tau)$) evaluated from the projected contours of PTD–MuG2 in dilute toluene solutions. τ is the time lag.

and chlorobenzene, in which A_2 values are similar to that in toluene (Figure S4 and Table S1, Supporting Information). The conformational changes of the PTD–MuG2 chain based on the projected morphology are tracked over time (Figure 2b,c). Interestingly, the conformational transitions occur rapidly between structures with different number of loops, where the most probable conformation has two loops. This facile loop formation might be initially perceived as counterintuitive, but this would explain how and why cyclic polymers are readily prepared by selective bond-formation between two terminal ends of a polymer that are seemingly very far apart.[36] The in situ TEM movie further reveals that segmental chain dynamics such as bending, rotation, and elongation drive the conformational transitions (Figure S5, Supporting Information). This behavior implies that the PTD–MuG2 chains are in the semiflexible polymer regime.

We performed coarse-grained bead-spring MD simulations under implicit solvent conditions using a model chain mimicking the architecture of the PTD–MuG2 molecule to understand the origin of dynamic conformational changes (Supporting Information). The steric repulsion of the bulky dendrons is sufficient to obtain the experimentally observed semiflexible behavior, leading to a persistence length comparable to that of the PTD–MuG2 molecules, estimated through LPTEM, cryo-TEM, dry-state TEM, and AFM measurements (Table S2 and Figure S6, Supporting Information). We performed a parameter sweep of the strength of the interbead attraction (ε) and calculated the loop formation ratio of the chains projected on a 2D plane, which is a proxy for the conformations of the chains (Figure 2d). Noting that ε is equivalent to the solvent conditions in the implicit solvent MD simulations, Figure 2d provides information on how the chain conformation

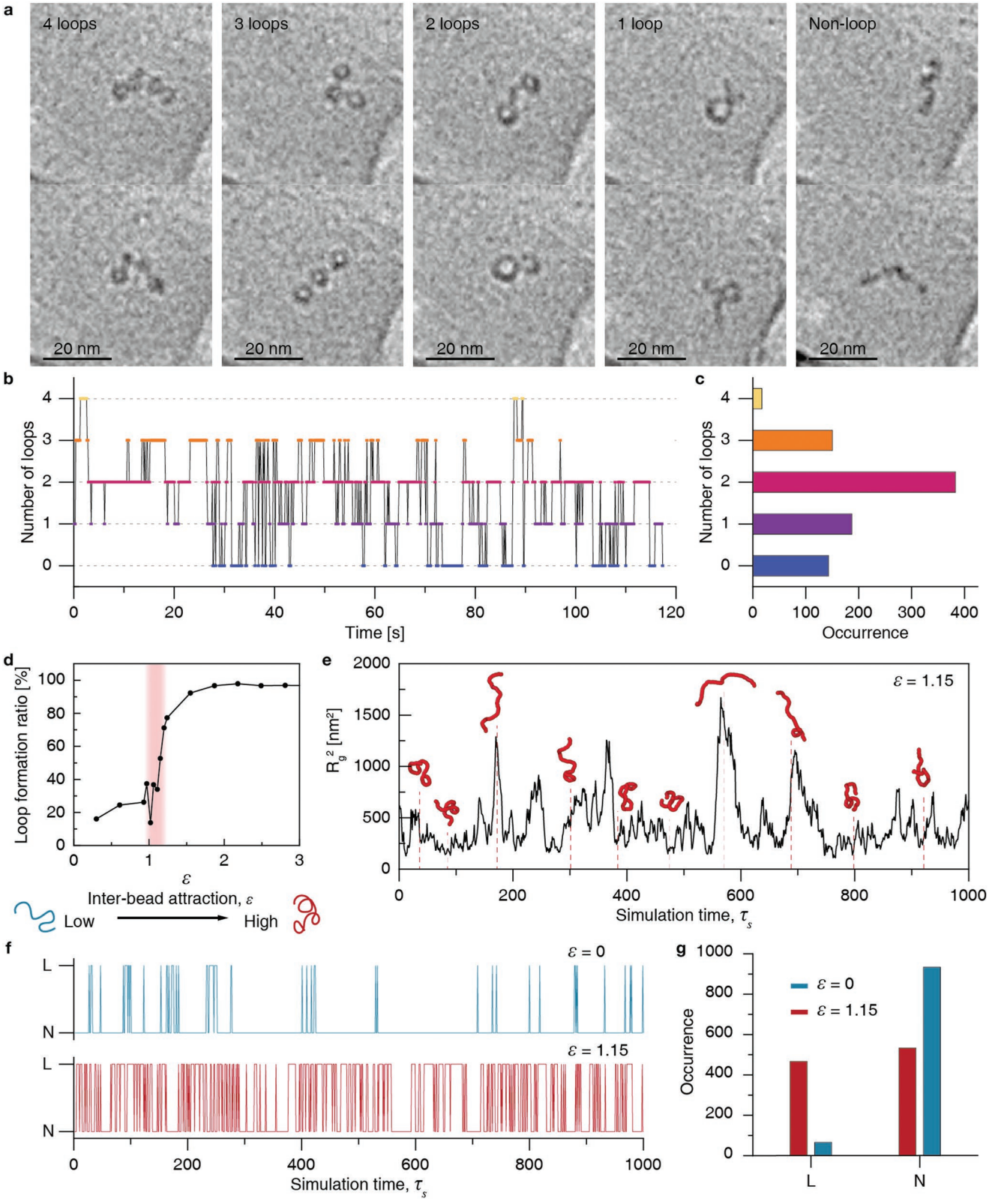

Figure 2. Dynamic conformational changes of a semiflexible polymer chain. a) Movie snapshots showing the conformational variation in PTD–MuG2 depending on the number of loops. b) Tracked conformational changes of PTD–MuG2 depending on the number of loops in projected contours. c) Histogram of the number of loops in the projected contours of PTD–MuG2 counted from (b). d) Loop formation ratio according to interbead attraction (ε) obtained from MD simulations: $\varepsilon = 0$ corresponds to purely repulsive intrachain interactions. e) $R_{g,proj.}^2$ over time and (inset) *xy* projection

changes as the solvent condition is modified. The results show a step-like transition behavior from stretched and non-looped conformations (low ε) to highly looped and collapsed structures (high ε). Interestingly, it is found that the dynamic behavior of the PTD–MuG2 chain with a selected interaction parameter (ε) of 1.15, representing dilute theta solvent where the intrachain interactions and thermal energy from the solvent induce vigorous structural fluctuations between the coiled and stretched shapes of the semiflexible polymers, exhibits dynamics similar to the polymer chain observed in LPTEM. The simulation trajectories are analyzed using the selected parameters. Simulation snapshots are projected onto the xy plane and temporally averaged over a short time interval to appropriately reproduce and compare with the contours obtained from LPTEM (Figure S7, Supporting Information). The resulting snapshots are shown as red contours, along with the time-dependent variations in the radius of gyration, in Figure 2e. Conformations of the chain include a variety of shapes, ranging from a triple-looped structure to a fully stretched coil; this highlights the dynamic structural fluctuation in the theta solvent. Compared to the single chain in a good solvent ($\varepsilon = 0.0$), conformational transitions and structural diversities are significantly enhanced in the theta solvent (Figure 2f,g). The MD simulation results (Figure 2d–g) suggest that the dynamic transition between the looped and non-looped conformations observed by LPTEM could be a natural consequence of the intrachain interactions of a semiflexible chain dissolved in a dilute theta solvent; which is governed only by the persistence length and the solvent quality.

2.3. Interactive Motions of Single Polymer Chains at the Gas–Liquid Interfaces and Graphene Substrates

It is expected that the observed semiflexible chain behavior is easily perturbed by interactions with the local, surrounding environment. Graphene liquid cell TEM allows for the observation of non-equilibrium single-chain dynamics at the gas–liquid interface and in the vicinity of the graphene surface (Movies S2–S5, Supporting Information). In general, bubbles can be generated by electron-beam-induced radiolysis of solvents in LPTEM observations. The generated bubble in Movie S2, Supporting Information, bounces to the right with slight expansion (Figure S8, Supporting Information). The interactive motions of a linear polymer chain at the gas–liquid interface are tracked along with the directional movement of the gas–liquid interface (**Figure 3**). Interestingly, one end of the polymer chain is anchored to this interface (Figure 3a), while the remainder of the chain moves in the same direction as the interface movement (Figure 3b,c). This is similar to the situation in low-grafting density, showing significantly different features from that of free-diffusing chains. The mean squared displacement (MSD) of the chain, calculated from the center-of-mass trajectories (Figure 3c), indicates that the pinned polymer chain exhibits directed motions with diffusion exponents of 1.28; this is higher than the value of 1 for normal diffusion (Figure 3d). This means that the chain is dragged by the gas–liquid interface. While being dragged, the pinned polymer chain usually retains a particular racquet-shaped conformation consisting of a line component and a single-loop component (Figure 3e and Figure S9, Supporting Information). The line portion of the chain hanging at the interface continuously stretches along the direction normal to the interface and swings along the direction of the interface fluctuation; meanwhile, the other component maintains its single-loop morphology. This local conformational heterogeneity within a single chain is probably due to the competition between the intrinsic bending stiffness of the chain and the local interfacial interaction induced by anchoring. The condition in high-grafting density is also observed, showing that the polymer chains interact with each other to behave like brush (Figure S10 and Movie S6, Supporting Information).

Fortunately, the direct observation of the present study enables the capture of a rare event where both ends of a single polymer chain are pinned at the gas–liquid interface, which eventually leads to chain scission; this is described in a time-series of TEM images and corresponding illustrations (Figure 3f,g). In this case, the overall behavior of the polymer is governed by interfacial interactions instead of intrachain interactions. The chain initially exhibits a double-loop conformation, consistent with its conformational dynamics when free from the interface (Figure 2c), and drifts freely in the liquid phase. When the chain approaches the gas–liquid interface, its conformation rapidly becomes unstable, followed by the anchoring of its two ends to the interface. As the two anchored ends fluctuate independently, the polymer chain is continuously stretched, resulting in cleavage at its midpoint owing to the accumulated tension. The force applied to the chain is likely due to the surface tension of the gas–liquid interface, which is large enough to induce chain cleavage (Supporting information). This phenomenon is analogous to polymer scission by bubbles, where a chain is pulled during the bursting or the collapse of bubbles until it is cleaved down the middle.[32,37] This is believed to be an important finding showing that mechanically induced chain cleavage can occur at the interface of bubbles without collapse or bursting of bubbles. After this chain breakage, the resultant two chains, each with one end anchored to the gas–liquid interface, behave similarly to those in the present work (as shown in Figure 3a), sometimes exhibiting a racquet-like conformation.

Depending on their functional groups and surface characteristics, polymers are known to interact with solid substrates.[38] The preferred looped conformation of the free-diffusing PTD–MuG2 chain is likely to enhance its interaction with solid substrates. It is also noted that the chain behavior is altered when it interacts with the graphene substrate in a liquid cell. The polymer chains often display structures restricted to a distinct conformation with multiple loops for an extended period of time, as shown in **Figure 4**a,b. For example, the two polymer chains shown in Figures 4c,d maintain double-loop and triple-loop conformations, respectively, for a while. In addition, there

images showing dynamic transitions between chain morphologies (stretched coils to multiple loops) obtained from a simulated semiflexible polymer with $\varepsilon = 1.15$. f) Tracked conformational transitions between looped (labeled L) and non-looped (labeled N) shapes in the projected conformations of a semiflexible polymer with $\varepsilon = 0$ (blue) and $\varepsilon = 1.15$ (red), respectively. g) Histogram of the number of L and N shapes counted from (f).

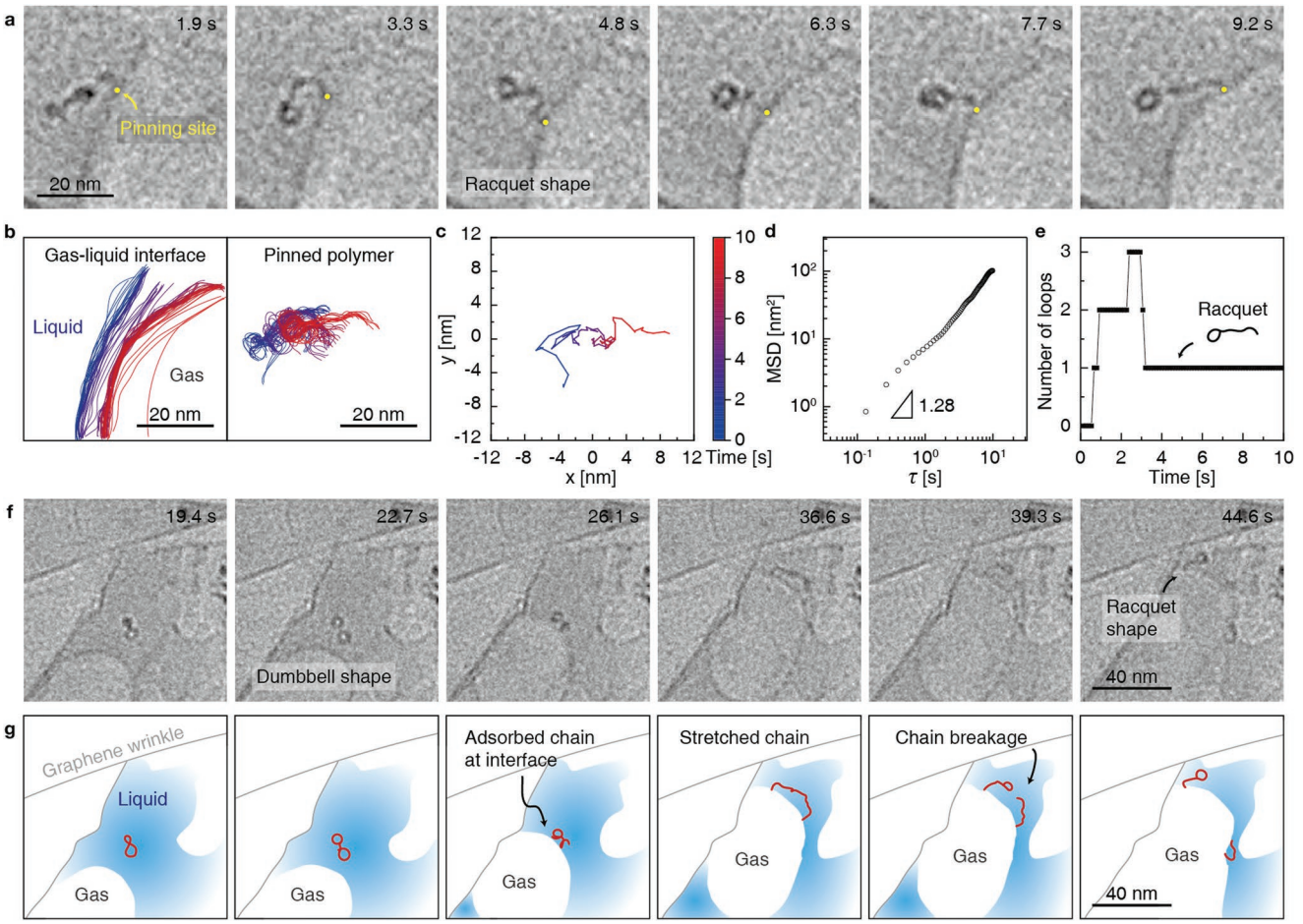

Figure 3. Interactive motions of linear polymer chains at the gas–liquid interface. a) Time-series of TEM images of the single-end anchoring of a polymer chain at the gas–liquid interface. The yellow dot indicates the pinning site. b) Superimposed trajectories of the gas–liquid interface with directional motion and the pinned polymer chain contours over 10 s. c) Center-of-mass trajectories of the pinned polymer chain over 10 s. d) MSD of the center-of-mass position of the pinned polymer chain. τ is the time lag. e) Tracked conformational changes of the pinned polymer chain depending on the number of loops in its projected conformation. f,g) Time-series of TEM images (f) and the corresponding schematics (g) of bubble-induced polymer chain scission.

is a period in which the change in the overall dimension of the distinct conformation is marginal, as seen in the tracked radius of gyration and the contour length (Figure 4e,f). This time period is longer than the relaxation time of the diffusing polymer chain (Figure 1i). This is probably due to the intermolecular interactions between the aromatic groups of the Müllen dendrons and graphene used as the window material for the liquid cell. Such interactions between the aromatic groups of polymers and substrates have been widely reported. One particular example is polystyrene phenyl groups which strongly interact with graphene by an effective π–π interaction.[39,40] In our study, the dense aromatic groups of the Müllen dendrons have partially weak attractive interactions with graphene, possibly influencing the temporal conformation and dynamics of the chain (Figure 4g).

3. Conclusion

Visualization of polymer structure and dynamics at the molecular level is of importance in current polymer science and engineering.[33,41,42] Tracking diverse dynamic molecular processes in situ and real-time requires high-speed imaging capabilities. In this study, we present the vivid visualizations of individual diffusing polymer chains in real time and in real space. Specifically, LPTEM observations of linear polymers with bulky aromatic dendrons in graphene liquid cells reveal distinct backbone conformational changes of these semiflexible polymers at the nanoscale. Our results show that intrachain interactions induce dynamic conformational fluctuations between coiled and stretched conformations. Visualizing how chain conformation changes in specific solvent conditions can provide an important insight in polymer engineering, such as the use of semiflexible polymer as scaffolds. Moreover, these chain behaviors differ greatly depending on the local environment. The chain dynamics under non-equilibrium perturbations can potentially explained the response of various biopolymers, double-stranded DNAs, filaments, collagens, and cytoskeletal components, under mechanical action in living systems. This direct investigation of the conformational dynamics of polymers in a solution phase that we present will improve the fundamental understanding of macromolecular physical

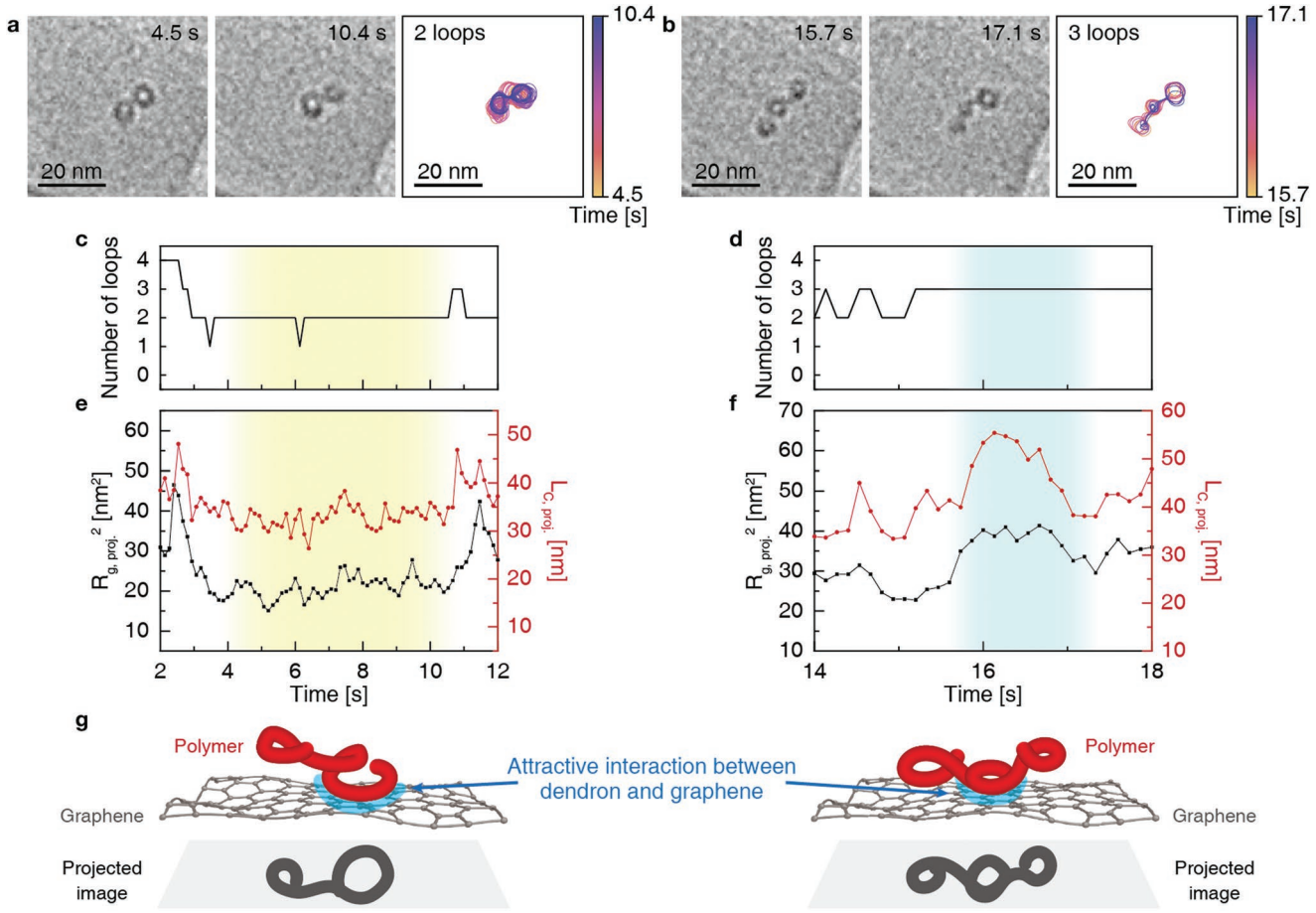

Figure 4. Restricted conformational dynamics of a single polymer chain. a,b) TEM images and superimposed trajectories of the chain contours of PTD–MuG2 showing restricted conformation. c,d) Tracked conformational changes of PTD–MuG2 depending on the number of loops in its projected conformation. e,f) $R_{g,proj.}^2$ and $L_{C,proj.}$ over time evaluated from the projected conformation. g) Schematics of the attractive interactions between Müllen dendrons and graphene. a,c,e) For double-loop shape; b,d,f) for triple-loop shape.

properties at the single-molecule level. In addition, recent advances in the state-of-art detecting system in TEM will further advance LPTEM as a powerful in situ visualization technique, equipped with sufficient spatiotemporal resolution, for soft materials in various types of solvents.[43,44]

4. Experimental Section

LPTEM: In situ TEM observations of the single polymer chain in graphene liquid cells were performed on a JEM-2100F (JEOL, Japan) instrument operated at 200 kV and equipped with an UltraScan 1000XP CCP detector (Gatan). Further, in situ TEM movies were recorded at 7.5 fps. The dose rate of the electron beam was maintained at 400 e^- Å^{-2} s^{-1}. In situ TEM observation in Figure S9b, Supporting Information, was performed on a JEM-ARM200F microscope (JEOL, Japan) installed at the National Center for Inter-University Research Facility (Seoul National University, Seoul, Korea). The microscope was equipped with an aberration corrector in the objective lens and an OneView IS camera (Gatan, USA) and operated at 200 kV.

Cryo-TEM: The synthesized polymer was diluted in toluene to a concentration of 10^{-5} mg mL^{-1} to observe single-chain conformations. A drop of the polymer solution was applied to the carbon side of the lacey carbon TEM grids, which was then blotted on one side for 10 s and plunge-frozen in liquid nitrogen with a Cryo-plunger 3 device (Gatan). This procedure embedded the polymer in a thin layer of amorphous ice. Cryo-TEM observations were performed on a JEM-2100F (JEOL, Japan) instrument operated at 200 kV and equipped with an UltraScan 1000XP CCP detector (Gatan). Images were obtained with a defocus value in the range of –1 to –2 µm. The accumulated total dose per image was less than approximately 50 e^- Å^{-2}.

Supporting Information

Supporting Information is available from the Wiley Online Library or from the author.

Acknowledgements

Y.B., M.Y.H., and K.-T.B. contributed equally to this work. This work was supported by the Institute for Basic Science (IBS-R006-D1). Y.B., J.K., J.S., S.K., D.K., and J.P. acknowledge the financial support from the NRF grant funded by the Korean government (MSIT) (NRF-2017R1A5A1015365 and NRF-2020R1A2C2101871), and Creative-Pioneering Researchers Program and Interdisciplinary Research Initiatives Programs by College of Engineering and College of Medicine, Seoul National University. J.P.

acknowledges the support from the Samsung Science and Technology Foundation under project number SSTF-BA1802-08 and POSCO Science Fellowship of POSCO TJ Park Foundation. T.-L.C. acknowledges the support from the Creative Research Initiative Grant through National Research Foundation of Korea. M.Y.H. and W.B.L. acknowledge the financial support from the NRF grant funded by the Korean government (MSIT) (NRF-2018M3D1A1058633, NRF-2019R1A2C1085081, and NRF-2020M3F7A1094299).

Conflict of Interest

The authors declare no conflict of interest.

Data Availability Statement

The data that support the findings of this study are available from the corresponding author upon reasonable request.

Keywords

conformational dynamics, dendronized polymers, semiflexible chain, single-chain dynamics, single-molecule imaging

Received: March 14, 2022
Revised: June 16, 2022
Published online:

[1] E. Helfand, Z. R. Wasserman, T. A. Weber, *J. Chem. Phys.* **1979**, *70*, 2016.
[2] E. Helfand, Z. R. Wasserman, T. A. Weber, *Macromolecules* **1980**, *13*, 526.
[3] M. P. Taylor, W. Paul, K. Binder, *J. Chem. Phys.* **2009**, *131*, 114907.
[4] P. E. Wright, H. J. Dyson, *Nat. Rev. Mol. Cell Biol.* **2015**, *16*, 18.
[5] R. Freeman, M. Han, Z. Álvarez, J. A. Lewis, J. R. Wester, N. Stephanopoulos, M. T. McClendon, C. Lynsky, J. M. Godbe, H. Sangji, E. Luijten, S. I. Stupp, *Science* **2018**, *362*, 808.
[6] M. F. Mabesoone, A. R. Palmans, E. W. Meijer, *J. Am. Chem. Soc.* **2020**, *142*, 19781.
[7] H. Cui, Z. Chen, S. Zhong, K. L. Wooley, D. J. Pochan, *Science* **2007**, *317*, 647.
[8] C. J. Hawker, K. L. Wooley, *Science* **2005**, *309*, 1200.
[9] G. H. Fredrickson, E. Helfand, *J. Chem. Phys.* **1990**, *93*, 2048.
[10] C. E. Sing, A. Alexander-Katz, *Macromolecules* **2011**, *16*, 6962.
[11] N. E. Moe, M. D. Ediger, *Macromolecules* **1995**, *28*, 2329.
[12] K. L. Ngai, R. W. Rendell, *J. Non-Cryst. Solids* **1991**, *131*, 942.
[13] R. C. Bernardi, M. C. Melo, K. Schulten, *Biochim. Biophys. Acta, Gen. Subj.* **2015**, *1850*, 872.
[14] M. P. Taylor, W. Paul, K. Binder, *Polym. Sci. Ser. C* **2013**, *55*, 23.
[15] T. Li, X. Yang, E. Nies, *J. Chem. Theory Comput.* **2011**, *7*, 188.
[16] M. Feig, I. Yu, P. H. Wang, G. Nawrocki, Y. Sugita, *J. Phys. Chem. B* **2017**, *121*, 8009.
[17] L. I. Klushin, A. M. Skvortsov, *J. Phys. A: Math. Theor.* **2011**, *44*, 473001.
[18] L. Wang, Z. Wang, R. Jiang, Y. Yin, B. Li, *Soft Matter* **2017**, *13*, 2216.
[19] L. C. Pierce, R. Salomon-Ferrer, C. Augusto, F. de Oliveira, J. A. McCammon, R. C. Walker, *J. Chem. Theory Comput.* **2012**, *8*, 2997.
[20] Y. F. Dufrêne, T. Ando, R. Garcia, D. Alsteens, D. Martinez-Martin, A. Engel, C. Gerber, D. J. Müller, *Nat. Nanotechnol.* **2017**, *12*, 295.
[21] H. G. Hansma, J. Vesenka, C. Siegerist, G. Kelderman, H. Morrett, R. L. Sinsheimer, V. Elings, C. Bustamante, P. K. Hansma, *Science* **1992**, *256*, 1180.
[22] M. Ganji, I. A. Shaltiel, S. Bisht, E. Kim, A. Kalichava, C. H. Haering, C. Dekker, *Science* **2018**, *360*, 102.
[23] M. Keshavarz, H. Engelkamp, J. Xu, E. Braeken, M. B. Otten, H. Uji-i, E. Schwartz, M. Koepf, A. Vananroye, J. Vermant, R. J. M. Nolte, F. De Schryver, J. C. Maan, J. Hofkens, P. C. M. Christianen, A. E. Rowan, *ACS Nano* **2016**, *10*, 1434.
[24] M. Abadi, M. F. Serag, S. Habuchi, *Nat. Commun.* **2018**, *9*, 5098.
[25] J. M. Chan, A. C. Kordon, R. Zhang, M. Wang, *Proc. Natl. Acad. Sci. USA* **2021**, *118*, e2109534118.
[26] Y. Zhou, K. W. Hsiao, K. E. Regan, D. Kong, G. B. McKenna, R. M. Robertson-Anderson, C. M. Schroeder, *Nat. Commun.* **2019**, *10*, 1753.
[27] K. H. Nagamanasa, H. Wang, S. Granick, *Adv. Mater.* **2017**, *29*, 1703555.
[28] S. Keskin, N. de Jonge, *Nano Lett.* **2018**, *18*, 7435.
[29] H. Cho, M. R. Jones, S. C. Nguyen, M. R. Hauwiller, A. Zettl, A. P. Alivisatos, *Nano Lett.* **2017**, *17*, 414.
[30] J. W. Smith, Q. Chen, *J. Mater. Chem. B* **2020**, *8*, 8490.
[31] B. A. Hammer, R. Moritz, R. Stangenberg, M. Baumgarten, K. Müllen, *Chem. Soc. Rev.* **2015**, *44*, 4072.
[32] G. I. Peterson, K. T. Bang, T. L. Choi, *J. Am. Chem. Soc.* **2018**, *140*, 8599.
[33] L. R. Parent, K. Gnanasekaran, J. Korpanty, N. C. Gianneschi, *ACS Macro Lett.* **2021**, *10*, 14.
[34] S. Kang, J. H. Kim, M. Lee, J. W. Yu, J. Kim, D. Kang, H. Baek, Y. Bae, B. H. Kim, S. Kang, S. Shim, S.-J. Park, W. B. Lee, T. Hyeon, J. Sung, J. Park, *Sci. Adv.* **2021**, *7*, eabi5419.
[35] A. Verch, M. Pfaff, N. de Jonge, *Langmuir* **2015**, *31*, 6956.
[36] F. M. Haque, S. M. Grayson, *Nat. Chem.* **2020**, *12*, 433.
[37] R. F. Hariadi, E. Winfree, B. Yurke, *Proc. Natl. Acad. Sci. USA* **2015**, *112*, E6086.
[38] M. Rubinstein, R. H. Colby, *Polymer physics*, Oxford University Press, New York **2003**.
[39] Y. Hong, S. Bao, X. Xiang, X. Wang, *ACS Macro Lett.* **2020**, *9*, 889.
[40] A. Rochefort, J. D. Wuest, *Langmuir* **2009**, *25*, 210.
[41] J. Chung, A. M. Kushner, A. C. Weisman, Z. Guan, *Nat. Mater.* **2014**, *13*, 1055.
[42] D. J. Mai, C. M. Schroeder, *ACS Macro Lett.* **2020**, *9*, 1332.
[43] W. Kühlbrandt, *Science* **2014**, *343*, 1443.
[44] G. M. Jonaid, W. J. Dearnaley, M. A. Casasanta, L. Kaylor, S. Berry, M. J. Dukes, M. S. Spilman, J. L. Gray, D. F. Kelly, *Adv. Mater.* **2021**, *33*, 2103221.

